Comprehensive metabolomics of the experimental opisthorchiasis

Kokova, D.

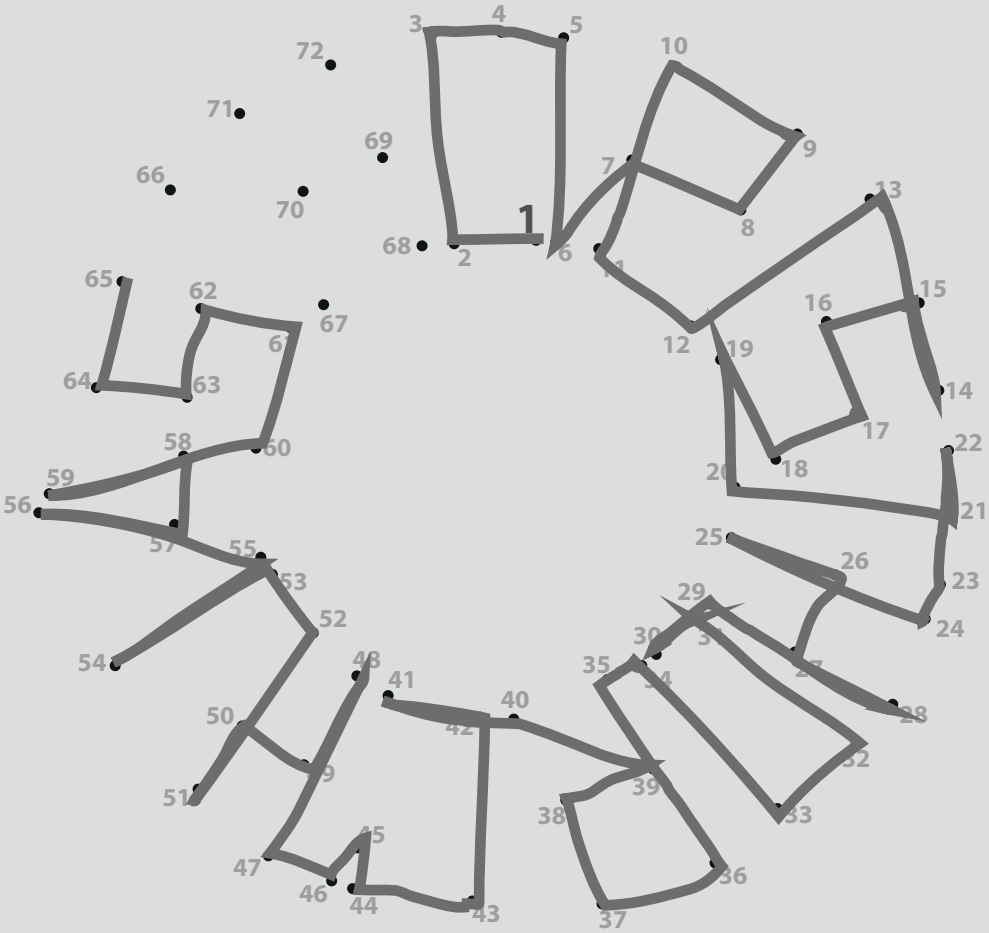
1
2
3
4
5
6
7
8
9
10
11
12
13
14
15
16
17
18
19
20
21
22
23
24
25
26
27
28
29
30
31
32
33
34
35
36
37
38
39
40
41
42
43
44
45
46
47
48
49
50
51
52
53
54
55
56
57
58
59
60
61
62
63
64
65
66
67
68
69
70
71
72

6

Metabolic homeostasis in chronic helminth infection is sustained by organ specific metabolic rewiring

D. Kokova
A. Verhoeven
E.A. Perina
V.V. Ivanov
M. Heijink
M. Yazdanbakhsh
O.A. Mayboroda

ACS Infect. Dis. 7:4 (2021)
https://doi.org/10.1021/acsinfecdis.1c00026

Abstract

Opisthorchiasis, is a hepatobiliary disease caused by flukes of the trematode family *Opisthorchiidae*. A chronic form of the disease implies a prolonged coexistence of a host and the parasite. The pathological changes inflicted by the worm to the host's hepatobiliary system are well documented. Yet, the response to the infection also triggers a deep remodeling of the host systemic metabolism reaching a new homeostasis and affecting the organs beyond the worm location. Understanding the metabolic alternation in chronic opisthorchiasis, could help us pinpoint pathways that underlie infection opening possibilities for the development of more selective treatment strategies. Here, with this report we apply an integrative, multicompartment metabolomics analysis, using multiple biofluids, stool samples and tissue extracts to describe metabolic changes in *O. felineus* infected animals at the chronic change. We show that the shift in lipid metabolism in the serum, a depletion of the amino acids pool, an alteration of the ketogenic pathways in the jejunum and a suppressed metabolic activity of the spleen are the key features of the metabolic host adaptation at the chronic stage of *O. felineus* infection. We describe this combination of the metabolic changes as a "metabolically mediated immunosuppressive status of organism" which develops during a chronic infection. A prolonged status of the immuno-hibernation might be one of the factors which increases risk of the infection related malignancy.

Significance Statement

A chronic helminths infection triggers a deep remodeling of the host systemic metabolism reaching a new homeostasis. Applying an integrative, multicompartment metabolomics analysis we show that the key features of the metabolic host adaptation at the chronic stage of *O. felineus* infection are the shift in lipid metabolism in the serum, a depletion of the amino acids pool, an alteration of the ketogenic pathways in the jejunum and most importantly a suppressed metabolic activity of the spleen. The metabolic patterns described here give a new insight into the host-parasite interaction. Finally, a simultaneous profiling of the metabolic signatures in the body fluids and the key metabolic organs helps spotting the potential metabolic vulnerabilities that might be targeted therapeutically.

Introduction

Opisthorchiasis a hepatobiliary disease is caused by flukes of the trematode family *Opisthorchiidae*: *Opisthorchis felineus* (*O. felineus*), *Opisthorchis viverrini* (*O. viverrini*) and *Clonorchis sinensis* (*C. sinensis*). Together, these three species affect more than 45 million people in endemic regions [1, 2]. The clinical manifestations of acute opisthorchiasis are non-specific and its chronic form usually appears asymptomatic [3, 4]. Yet, at chronic stage of infection, there is progressive accumulation of pathological changes in the host due to egg induced fibrosis and the local damage inflicted to the biliary epithelium by the worms. Moreover, a long-term coexistence with a parasite leads to a remodeling of the host systemic metabolism. How and at what cost this new homeostasis is sustained is still poorly understood, but a current theoretical framework [5] implies that metabolic shift has a profound influence on the host immune status and eventually affects the organs that are not directly involved in the immune response. Understanding the metabolic alternation in opisthorchiasis, could help us understand pathways that underlie infection and disease progression that might be targets of therapeutics.

Metabolomics technology offers a method for exploring of the systemic metabolism. Today, metabolomics of helminth infections is an area of active research. It has been shown that metabolic response of the host usually leads to changes in the pattern of amino acids in the body fluids, remodeling of the lipid metabolism and changes in composition of the microbiota-related metabolites [6]. Yet, while metabolic responses to helminth infections in animal models are rather strong and easily detectable, the field studies with human participants have shown that these infections are not one of the strongest factors that can influence the metabolic composition of body fluids. The traditional confounding factors such as age, gender, BMI, and lifestyle mask the infection related metabolic adaptations [7]. Of course, one of the main differences of the field studies with the animal experiments is the degree of control over the sources of the unwanted variance. Another difference is that animal studies often report only the effects observed at the early stage of the infection, while in the "real life" situation, it is

the chronic stages of infection that we are likely to encounter.

Recently, using an experimental infection system with a liver fluke O. felineus we have shown that in urine and blood the metabolic response stabilizes after the 12th week of infection and hardly any statistically significant changes can be found between infected and uninfected animals [8, 9]. Here to emulate the chronic stage of infection data are generated over twenty weeks post infection. Moreover, the systemic changes in the metabolism are not expected to be limited to the serum or urine but could affect multiple organs and functional systems of an organism. Therefore, for the first time a multicompartment approach were used for a detailed description of the metabolic phenotype of the chronic helminth infection, beyond the conventionally used biofluids (blood, urine). The choice of compartments was guided by the current views on parasite biology and published studies on the morbidities associated with opisthorchiasis. To this end we analyzed serum, urine, and stool samples in addition to the organs, liver, spleen, gut (jejunum, ileum, and colon) and the kidneys. The liver, where the flukes reside, the three segments of intestine: jejunum, ileum, and colon where the eggs of the flukes are usually pass and can get trapped in granulomas, as well as the spleen, the largest part of the lymphatic system involved in the immune response of a host to a parasite infection [10, 11]. It has been shown that opisthorchiasis leads to nephropathy, thus the kidney – one of the key metabolic organs was also included in our analysis [12, 13]. Finally, not only have we looked at the metabolomics using NMR but we have also used the quantitative gas chromatography-mass spectrometric profiling of fatty acids in peripheral blood with the view to the role that lipid metabolism plays in a host response to an infection. Every compartment delivers an independent set of the data, which we refer to as "data blocks". In total, eleven data blocks corresponding to each of the sample types were generated and analyzed (Figure 1).

Thus, with this report we for the first time apply an integrative analysis, using multiple biofluids and tissue extracts to describe metabolic changes in O. felineus infected animals at the chronic change. We show that the shift in lipid metabolism in the serum and the changes in the spleen metabolism are the key features of the metabolic host adaptation at the chronic stage of *O. felineus* infection.

Results

Outline of the experiment, basic animal characteristics, histology, and metabolite quantification

Figure 1 summarizes our experimental design: an observational study with two (infected vs. non-infected) experimental equally sized experimental groups. One animal deceased before the end of the experiment, thus our final sample consists of 19 animals: 10 controls (5 females and 5 males) and 9 infected animals (4 females and 5 males). At the end of the experiment, the median body weight of the animals in the control and infected group was 133.85 and 118.20 grams, respectively, with no statistically significant difference. However, a gender specific comparison shows that body weight of the infected female animals is significantly lower than non-infected ones (p-value = 0.04). Similarly, liver weight shows no significant difference between the infected and non-infected group, while a gender specific comparison shows an increase in the liver weight for the infected male animals (p-value < 0.0001) (Supplementary Figure 1).

To obtain a representative overview of the metabolic differences between the infected and non-infected animals at twenty weeks post infection we collected the main biofluids (blood and urine), feces, the main metabolic organs (liver and kidney), three segments of the digestive tract (colon, ileum and jejunum) and the spleen. The histological analysis shows no difference between the segments of the digestive tract or the kidney of infected and uninfected groups. The liver samples of *O. felineus* infected animals had areas of inflammatory cell infiltration occurring around the bile ducts. The histological analysis of the liver samples of the control group showed no evidence of pathological changes in the liver or the bile ducts (Supplementary Figure 2).

For metabolomics analysis we took a quantitative targeted approach. Using the Chenomx NMR suite we quantified 22 metabolites in urine, 45 in liver, 39 in kidney, 37 in spleen and ileum, 33 in jejunum, 28 in colon samples, 24 in feces and 24 in the serum samples. Moreover, for serum nine resonances corresponding to the different parts of the serum lipoproteins were integrated (SI file data) and 38 short-, long- and very long-chain fatty acids in serum samples were

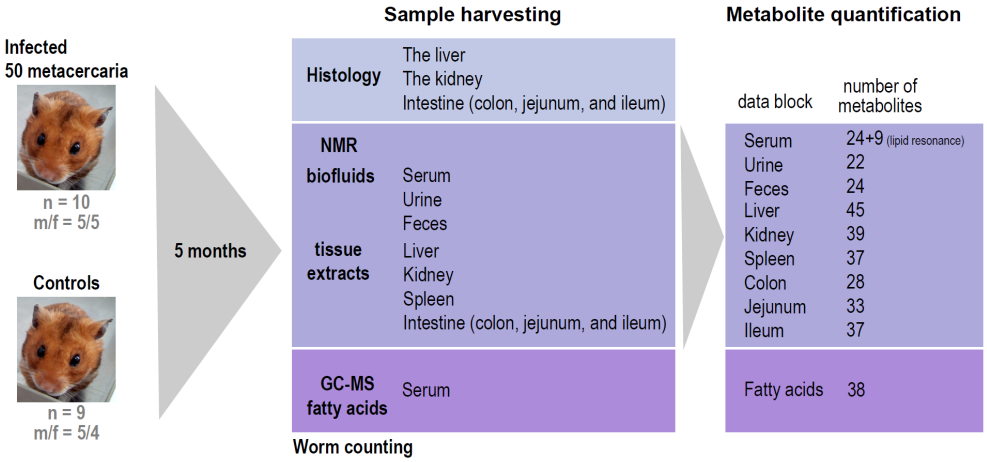

Figure 1. Study design. Twenty golden Syrian Hamsters (Mesocricetus auratus) of both genders were divided for two groups. Ten animals (five males and five females) were infected orally with 50 O. felineus metacercariae (Infected group). The remaining ten hamsters (five males and five females) were kept as a control group. During the experiment one female animal of the infected group died. Blood serum, urine, feces, liver, kidney, spleen, and intestine samples were collected in the 20th week post-infection from the animals of both groups for NMR, GC-MS and morphological analysis.

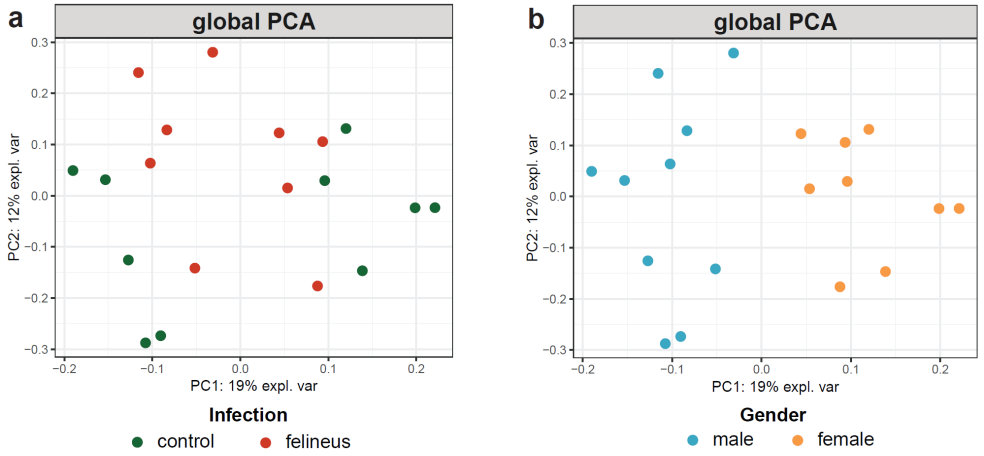

Figure 2. The scores plot of the observations on the first two kernel principal components (PCs) in global PCA model built on all datasets; a: colored by the infection status; b: colored by gender of an animal. The model shows that not the infection, but gender is the main source of variance in the combined model.

quantified using mass spectrometry. Only alanine and lactate were detected in all studied samples; tyrosine, valine, choline, phenylalanine, isoleucine, and leucine were found almost in all samples apart from urine. Creatine, glutamine, glutamate, uracil, fumarate, and glucose were quantified in all tissue samples. Supplementary Figure 3 summarizes the quantified metabolites across the samples.

Multi-block analysis and selection of the relevant data blocks

Figure 2 shows a score plot of the global PCA model built on all 11 data blocks using an unsupervised multiple kernel method [14]. The method enables an integrated overview of the major trends in the data. The model required 5 principal components (PC) to explain 56 % of the variance with 31% covered by the first two components. The score plot of the model shows that not the infection (Figure 2a) but gender (Figure 2b) is the main source of variance in the combined model. The gender-related clustering is associated with the strongest component of the combined model which explains 19% of the total variance (Figure 2). To estimate the relative contribution of each individual block to the variance associated with infection, we applied an unsupervised multi-block modeling approach with correction for the gender effect. A practical realization of such analysis is the Multi-Omics Factor Analysis (MOFA) algorithm [15]. The MOFA can be viewed as a generalization of PCA for multi-block problems, which obtains a set of latent factors capturing the major variation across multiple data sets. Figure 3 summaries the MOFA model built on 11 available blocks of data. The model converged to 10 factors, which cumulatively explain 77% of variation in the colon samples, 56% in the ileum, 56% in the jejunum, 70% in the liver, 77% in the spleen, 50% in the kidney, 71% in the urine samples, 65% in the stool, 69% in the serum, 70% in serum fatty acids, and only 8% in the lipoprotein block (Figure 3a). An overview of all factors (Supplementary Figure 4 and Figure 3b) shows that the latent factor 6 is aligned with the status of infection. Figure 3c shows the contribution of the individual data blocks to latent factor 6. It is evident that four blocks, namely the serum fatty acids (15% of the variance), the jejunum (13%), liver (12%) and spleen (12%) have strongest influence on the factor. Supplementary Figures 5-8 show the heat maps for the four selected blocks visualizing the weights of the individual metabolites on latent factor 6. However, even though the changes between the infected and non-infected animals can be identi-

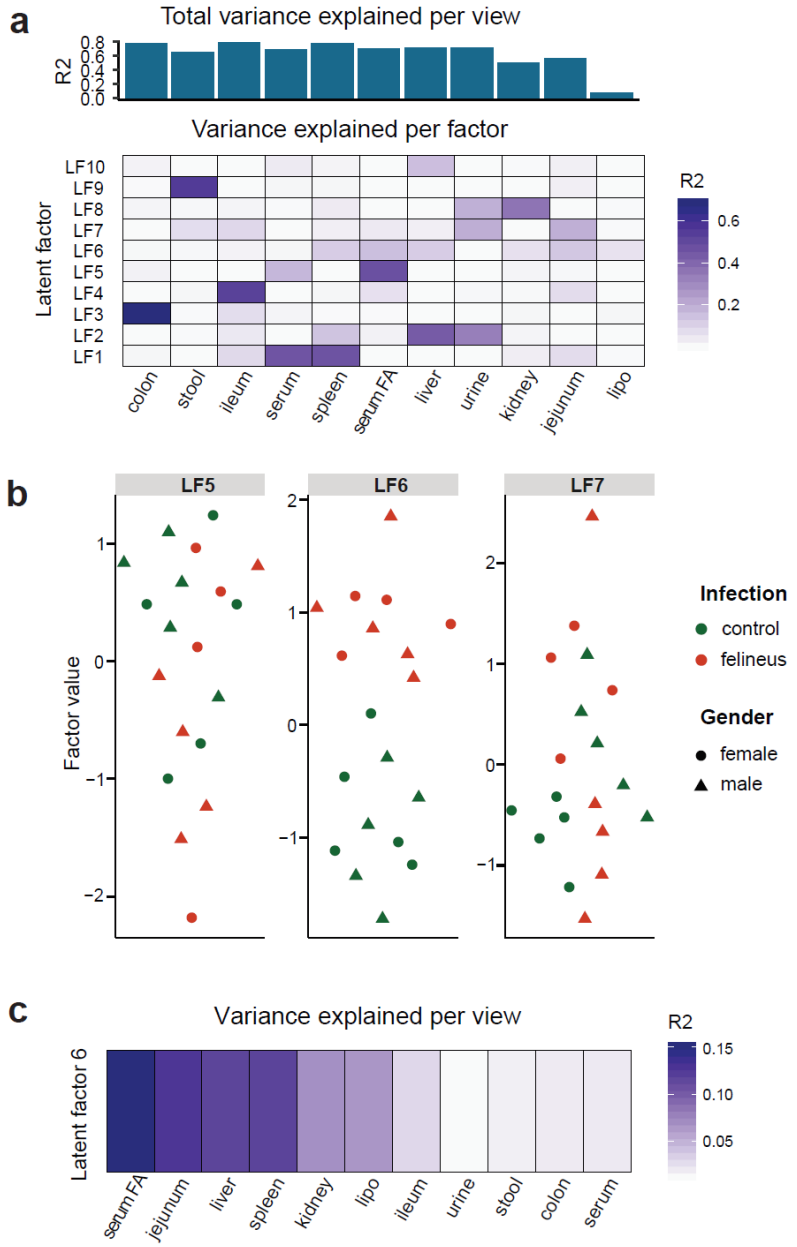

Figure 3. Multi-Omics Factor Analysis (MOFA) modeling. The model built on the 11 available blocks of data. a: cumulative proportion of total variance (R2) per block of the data and variance explained per factor in each data block; b: the swam plots showing the sample clustering along the factors values for the latent factors 5, 6 and 7; color shows infection status and shape – gender. c: representation of decomposition of variance (R2) in the latent factor 6 in each data block.

fied visually, a selection of the most relevant metabolites which could compose an "infection signature" requires a regression-based strategy.

Metabolic signature of chronic opisthorchiasis

Figure 4a shows the distribution of the individual samples along the first two component of the multiblock regression model. All datasets show clear clustering of two sample groups on the first component (covers 41.3% of variance in spleen data, 31.3% in liver, 27.8% in serum fatty acids, and 17.6% in jejunum). Figure 4b presents the variables in a clustered image map (Fig 4b) based on the Euclidean distance and complete linkage. It displays an unsupervised clustering between selected metabolites of spleen, liver, jejunum and serum fatty acids and the animals. Figure 4b presents all significantly increasing serum fatty acids in the infected animals; concentrations of inosine, lactate, myo-inositol, proline, sarcosine, theophylline, maltose, and carnitine are suppressed in the infected group, while liver uracil is increased; levels of methyl-histidine, leucine, citrate, in jejunum of O. felineus group are increased, while jejunum lactate and xanthine are decreased; and in spleen, the level of glutamine is lifted in presence of opisthorchiasis, when most metabolites are suppressed: ascorbate, alanine, myo-inositol, methionine, creatine, glutamate, fumarate, o-phosphocholine, and threonine. Figure 5 shows the correlation between the selected variables of the different blocks (correlation cut-off |0.7|). Remarkably, all serum fatty acids show negative correlations with the metabolites of the tissues. The liver metabolites, namely inosine, lactate, carnitine, sarcosine, proline, and maltose positively correlate with the spleen and jejunum. With exception of glutamine, all spleen metabolites show positive correlations with liver and jejunum and negative one with the fatty acids; yet ascorbate correlates only with jejunum xanthine and serum DGLA. Of the jejunum metabolites, only lactate and xanthine show correlation with other data blocks.

To access our model performance, we applied 5-fold cross-validation. Supplementary Table 1 summarizes the cross-validated AUC values and their respective p-values for each block. Finally, we used an unsupervised clustering approach to test the selected subset of metabolites. The Supplementary Figure 9 shows the results of a PCA plot of the K-means clusters built on the selected variables; the samples are clustered according to the infection status, which implies that the

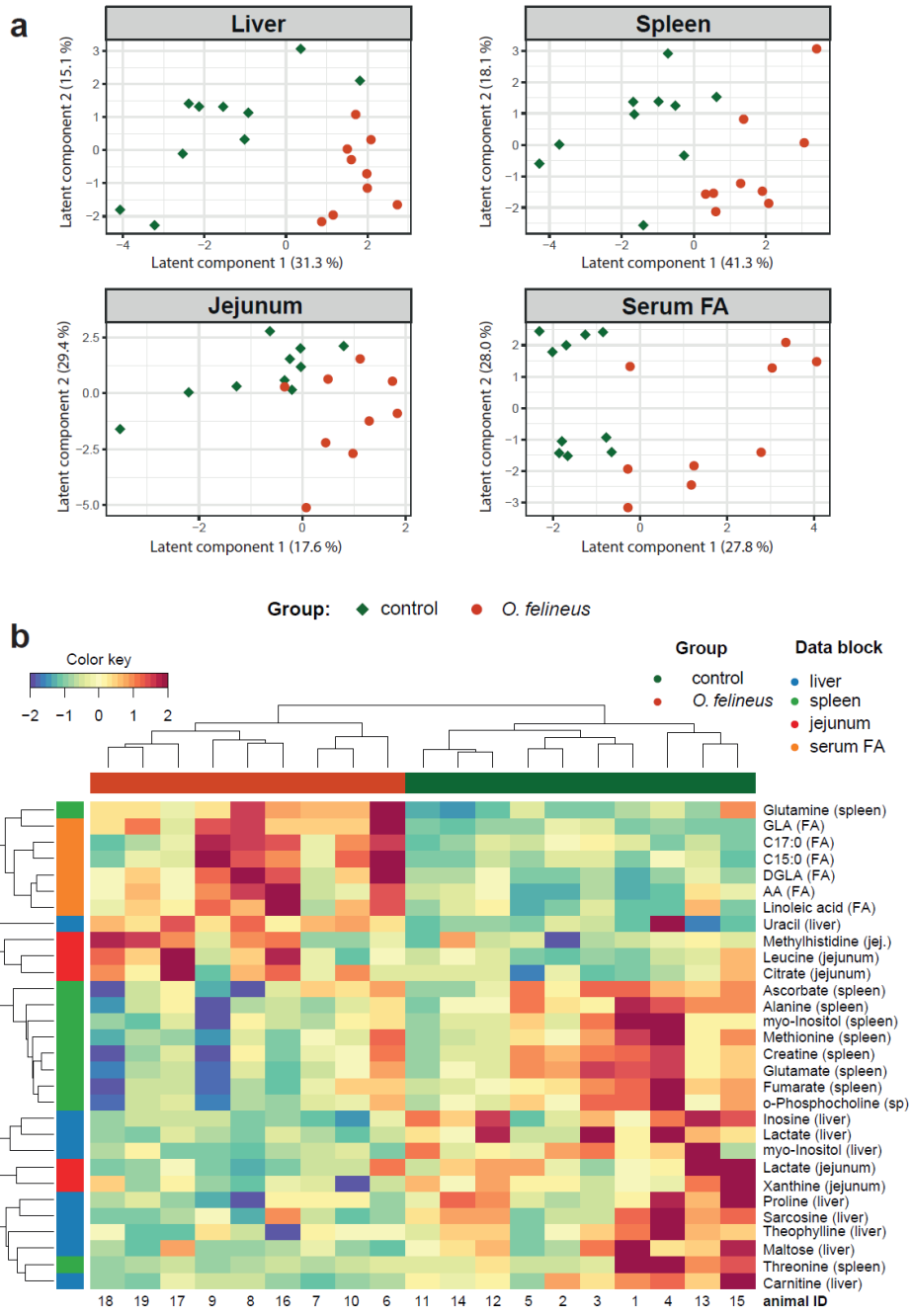

Figure 4. DIABLO modelling. a: Scores plots of each data blocks based on the first and the second components from the DIABLO model. b: A heat map built on the subset of the variables selected by a DIABLO model; the columns present the observations, the rows – the discriminating metabolites.

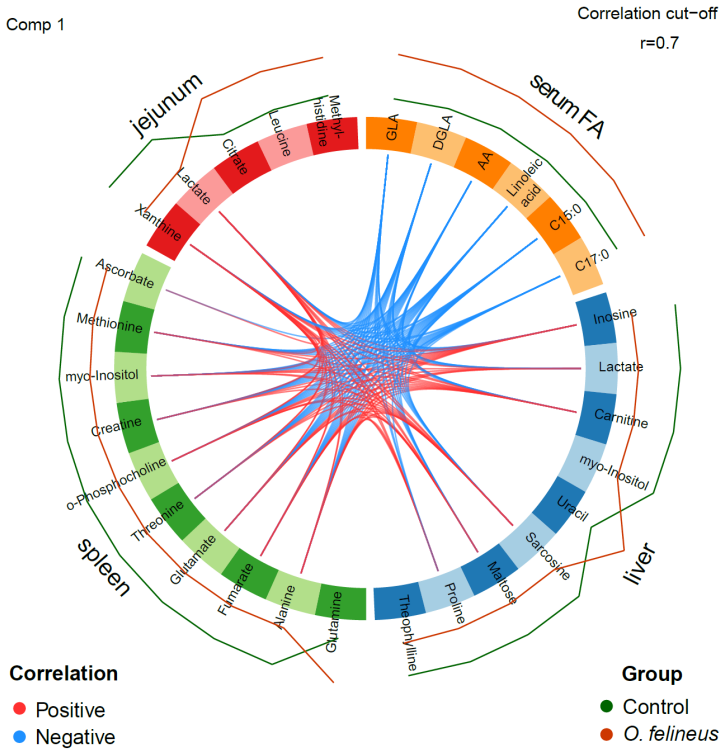

Figure 5. Plot represents the correlations (cut-off is 0.7) between variables of different blocks. All serum fatty acids show negative correlations with the metabolites of the tissues. With exception of glutamine, all spleen metabolites show positive correlations with liver and jejunum and negative one with the fatty acids. Of the jejunum metabolites, only lactate and xanthine show correlation with other data blocks.

samples within the clusters have similar metabolic characteristics.

Pathway enrichment analysis on the metabolic signature of chronic *O. felineus*-infection

To get insight into the metabolic networks which could be associated with the infection we used the MetExplore environment. MetExplore can map the selected subsets of the metabolites into the pathways using organism specific databases. To this end, we used for mapping a subset of the spleen metabolites: ascorbate, methionine, myo-inositol, creatine, o-phosphocholine, threonine, glutamate, fumarate, alanine, and glutamate. Seven significant pathways involving were 30 reactions (Table 1) were chosen based on the Bonferroni-corrected p-values. All metabolites, except o-phosphocholine,

were mapped into the sub-networks (Supplementary Figure 10). The mapping of the liver metabolites did not result in any significantly enriched pathways (p-value ≥ 0.05). For jejunum only leucine and citrate were significantly associated with 2-oxocarboxylic acid metabolism. Thus, a limited number of the metabolites included in the analysis certainly restricts the possibilities for interpretation. Yet, spleen data clearly point towards a dis-regulation in the glutathione, glutamate, and alanine balance.

Table 1. The result of the pathway enrichment analysis run on the metabolites selected by DIABLO multi-block modeling

Significant pathway	KEGG identifier	Number of metabolites	Corrected p-value
Spleen			
Biosynthesis of amino acids	cge01230	6	$2.4*10^{-5}$
Aminoacyl-tRNA biosynthesis	cge00970	5	$1.7*10^{-4}$
Alanine, aspartate, and glutamate metabolism	cge00250	4	$7.9*10^{-4}$
Arginine and proline metabolism	cge00330	4	$5.9*10^{-3}$
Glutamine and glutamate metabolism	cge00471	2	0.017
Nitrogen metabolism	cge00910	2	0.023
Ascorbate and aldarate metabolism	cge00053	2	0.049
Jejunum			
2-Oxocarboxylic acid	cge01210	2	0.02

Systemic balance of glutamine

It has been shown that an active infection process increases the catabolism of glutamine by the immune cells and as such changes the balance of glutamine, glutamine/glutamate and therefore the glutamine/alanine ratios [16]. The Figure 6 shows a comparative overview of glutamine balance for serum and all analyzed tissue samples. In agreement with existing data on the glutamine distribution its concentration in serum was higher than in the tissues, but there is no significant difference between serum concentrations of glutamine of the infected and non-infected animals. The glutamine/glutamate ratio is significantly lower in the liver of the infected animals (p-value = 0.02). The most consistent changes are observed in the spleen: the

concentration of glutamine (p-value = 0.0007) and corresponding glutamine/glutamate (p-value < 0.00001) and glutamine/alanine (p-value < 0.00001) ratios are higher in the spleen of the infected animals.

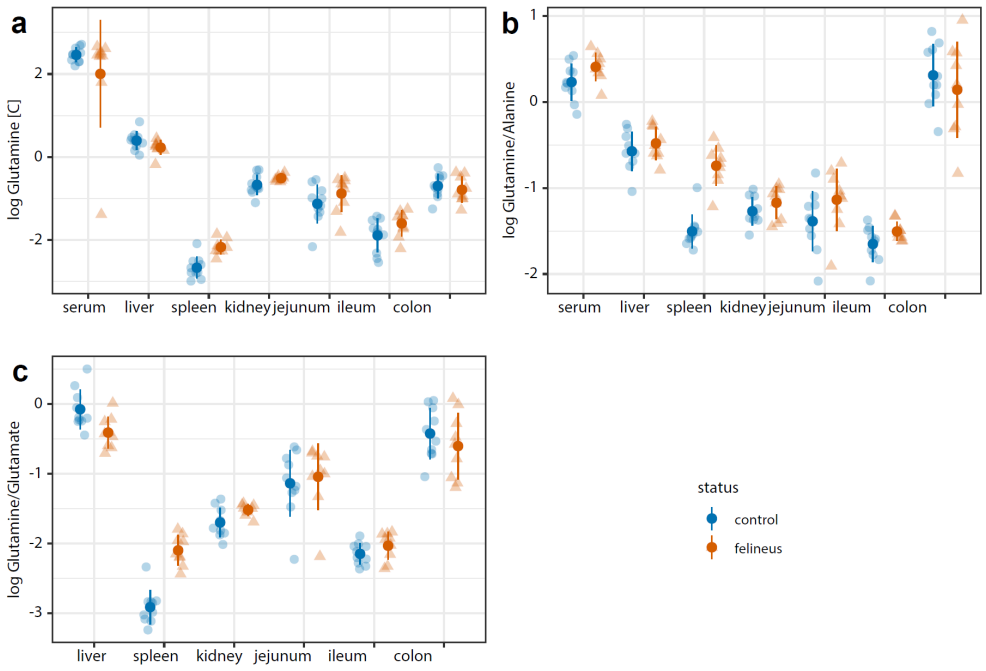

Figure 6. An overview of glutamine balance; a: glutamine. The glutamine concentration in serum was higher than in the tissues, but there is no significant difference of serum glutamine concentrations between the infected and non-infected animals. The most consistent changes are observed in the spleen (p-value = 0.0007). b: glutamine/alanine ratio. The glutamine/alanine ratio is higher in the spleen of the infected animals (p-value < 0.00001). c: glutamine/glutamate ratio. The glutamine/glutamate ratio is significantly lower in the liver tissue (p-value = 0.02) and higher in spleen tissue (p-value < 0.00001) for the infected animals. glutamine/glutamate (p-value < 0.00001).

Discussion

Metabolic phenotyping of the pathological conditions is often restricted to the most accessible types of biological samples such as urine, serum, and feces. Yet, the systemic changes in the metabolism are not limited to the serum or urine but affect multiple organs and functional systems of an organism. Thus, aiming for an extended study of the metabolic phenotype of the chronic *O. felineus* infection we analyzed the samples from the most relevant compartments in the body. We have generated eleven data blocks, each corresponding to the samples analyzed. A set of four - liver, spleen, jejunum, and serum fatty acids were needed to, as a whole, explain the variance of the data related to chronic infection with *O. felineus*. (Figure 3). Thus, we can conclude that with the exception of the serum fatty acids at the chronic stage of the infection metabolic composition of the biofluids in the infected and non-infected animals remains rather similar. This observation is in an agreement both with the reports on the human material [7] and our recent publication on the animal model [8, 9]. Indeed, the field studies on the human body fluids show that the traditional confounding factors such as age, gender, BMI, and lifestyle affect their metabolic composition more strongly than the infection and simply override the effect of infection. In our report of the animal model we have shown that the infection related metabolomic changes in urine are the most pronounced from the fourth week up to the 12th weeks post-infection. At later time points no significant differences between the infected and control animals were detected [8]. The same applies to serum metabolites, and serum lipoprotein clusters: the statistically significant changes in amino acids and lipid clusters were observed in the first weeks after the infection [9]. Only few metabolites remained marginally different beyond the tenth week of infection. Thus, the current results and our previous reports show that after initial state of the "metabolic stress" [8, 9] organism reaches a state of metabolic homeostasis. This homeostasis, however, is sustained by a shift in the systemic lipid metabolism and local, organ specific metabolic rewiring.

Indeed, here we indicate that the circulating serum fatty acids, liver, spleen, jejunum show the strongest contribution to the systemic

metabolic changes associated with chronic opisthorchiasis. While our analysis does not exclude a possibility that other body compartments may contribute, the ones we identified here appear essential for the description of the metabolic changes triggered by chronic *O. felineus* infection. Our results show that "integrated metabolic signature" of chronical opisthorchiasis consists of 30 structures associated with lipid, amino acid, and energy metabolism. Moreover, six serum fatty acids, glutamine in the spleen, uracil in the liver and methyl-histidine, leucine and citrate in jejunum form a cluster of compounds that are increased in the chronically infected animals. The remaining 22 metabolites are depleted in the chronically infected group. Thus, the most important metabolic features of the chronic *O. felineus* infection are the increase in the circulating serum fatty acids, depletion of the amino acids pool in liver, spleen and jejunum. We believe that the given pattern points towards a specific type of systemic metabolic adaptation.

Indeed, a subset of the free fatty acids contributing to the infection signature contains two odd-chain fatty acids (pentadecanoic and heptadecanoic acids) and a group of the functionally linked structures, namely LA, GLA, DGLA and AA. All those structures were reported having a reverse association with a risk of type 2 diabetes [17–19]. Moreover, all mentioned fatty acids are either essential or conditionally essential which implies their dietary origin, or as the recent report on C15:0 and C17:0 fatty acids showing, they can be produced by gut microbiota [20, 21] and therefore the characterization of the microbiome at the chronic stage of opisthorchiasis should shed light on this. This, in turn, makes it possible to suggest involvement of the microbiota in regulation of metabolic homeostasis during the chronic infection. Furthermore, a recently published meta-analysis of the metabolic markers of the pre-diabetic and diabetic subjects show that the increased concentrations of the BCAAs, aromatic amino acids, alanine, lactate and the glutamine/glutamate ratio in the blood is characteristic for these conditions [22]. In our report on the time-resolved metabolomics of serum samples during *O. felineus* infection, we observed the strong decrease of the BCAAs during the first weeks of infection [9]. Although the depletion of the circulating BCCAs stabilizes around the tenth week, their levels remain lower than controls for the 22 weeks of the entire experiment [9]. In the current report, the concentration of alanine in the infected animals was lower not only in the liver and spleen, the organs which contribute to the infection signature but also

in serum (Figure 6). Considering the data on a negative association between helminth infections and a risk of metabolic syndrome [23], one might be tempted to focus on the similarities between the changes in the systemic metabolism triggered by the chronic *O. felineus* infection and the "protective" metabolic patterns. Yet, the chronic infection with *O. felineus* increases the risk of liver pathologies and even cancer [24]; thus, we believe that the prolonged changes in the utilization of the main metabolic fuel components and the local depletion of the amino acids pool leads gradually to a physiological condition which can be labeled as a "metabolically driven immunosuppresion". For instance, we show that metabolic activity of the spleen is suppressed in the infected animals; our data show the increased concentrations of glutamine/glutamate and glutamine/alanine ratios in the spleen of the infected animals. This, in turn, implies a reduced conversion of glutamine to glutamate by glutaminase. The glutamine/glutamate ratio is often used for a rough assessment of the cell proliferation activity: a high ratio indicates a reduced consumption of glutamine and consequently lower proliferation rates within an organ [25]. It is worth of mentioning that in liver the glutamine/glutamate ratio is shifted in the opposite way, thus suggesting a higher metabolic activity of the liver of the infected animals. This is in agreement with the liver responses to the presence of the parasite, the adaptations to the mechanical damage of the biliary system, and the processes controlling the inflammation, eosinophilia and periductal fibrosis [26]. All those factors are probably responsible for the increased weight of the organ in the infected animals (Supplementary Figure 1). Finally, the pathway enrichment analysis suggests an alteration in the keto-acids pathways (2-oxocarboxylic acids metabolism) in jejunum, which is in agreement with the reported increased concentration of leucine (Supplementary Figure 11). Leucine is a strictly ketogenic amino acid, which implies that it is converted to the fat rather than glucose. Moreover, an active catabolism of leucine is essential for regulation of intestinal immune function [27] and regulation of the entire mTOR signaling system [28]. Thus, although the limited number of the metabolites that change upon chronic opisthorchiasis restricts our ability to draw firm mechanistic insights, they do indicate a local depletion of the amino acids pool, an alteration of the ketogenic pathways in the jejunum and last but not least a suppressed metabolic activity of the spleen. We can tentatively describe this combination of the metabolic changes a "met-

abolically mediated immunosuppressive status of organism" which develops during a chronic infection. A prolonged status of the immuno-hibernation might be one of the factors which increases risk of the infection related malignancy.

Materials and Methods

Ethics statement

All procedures with animals were carried out according to the recommendations of the national guidelines for animal caring: 12.08.1977 N 755 "On measures to further improve the organizational forms of work using experimental animals" and approved by the Siberian State Medical University (license number 5786 issued on 26.02.2018).

Parasites, experimental opisthorchiasis model and experimental design

Twenty golden Syrian Hamsters (Mesocricetus auratus) of both genders were purchased from the animal facility of the Institute of Bioorganic Chemistry Academicians M.M. Shemyakin and U. A. Ovchinnikov. The hamsters were housed in groups of five with provided food and water ad libitum for the duration of the experiment. After one week of acclimatization, ten animals (five males and five females) were infected orally with 50 O. felineus metacercariae in phosphate-buffered saline (PBS) of each hamster (Infected group). O. felineus metacercariae were obtained from naturally infected fishes captured from the Ob river in endemic areas of Tomsk, Russian Federation. The viable metacercariae were collected and identified by microscopy from the pepsin-HCl-digested muscular and subcutaneous tissues. The remaining ten hamsters (five males and five females) were subjected to the same procedures with PBS (control group). During the experiment one female animal of the infected group died.

Sample collection and assessment of the infection

Blood serum, urine, feces samples were collected in the 20th week post-infection from the animals of both groups. The hamsters were placed individually into sterile empty glass crates for collecting urine and feces, where separation of stool from urine was facilitated. The urine samples were collected into labeled cryotubes over ice and stored frozen at -80°C. 2-3 pellets of animal feces were collected into labeled cryotubes over ice and stored frozen at -80°C until NMR analysis.

On the day after collecting the biofluid samples, the animals were sacrificed, and tissue samples and serum were collected for NMR and morphological analysis. The blood samples were collected into vacutainer tubes (no additive), left on ice for coagulation, and centrifugated at 3500 g for 10 min. The provided serum was transferred into cryotubes and stored at -80°C. Small samples of the 3 intestinal parts (colon, jejunum and ileum), part of the liver, and the right kidney were transferred into 5 mL tubes containing a solution of 4% buffered formalin for subsequent histological analysis via hematoxylin and eosin staining. The left kidney and the spleen were harvested and transferred into a 2 mL cryotube, immediately immersed in liquid nitrogen and stored at -80 °C for NMR analysis. Small portions (~0.5 cm) of intestinal tissue (colon, jejunum and ileum) were cut from the middle of each section. Then, the intestinal tissue portions were washed with PBS, transferred into cryotubes, immersed in liquid nitrogen, and stored at -80 °C for NMR analysis. The rest of the liver from infected animals after collecting histological material, was treated over ice to remove flukes from the bile ducts. The liver then was collected into the cryotubes, immersed in liquid nitrogen, and stored at -80 °C. The liver from control group of animals was treated by the same procedure as the liver of infected animals.

Assessment of the infection intensity was performed by counting worms in the liver and bile ducts for each infected hamster.

Sample preparation for NMR data acquisition

All chemicals used for the buffer solutions were purchased from Sigma-Aldrich except for the 2H2O (Cortecnet) and the 3-(trimethylsilyl)propionic-2,2,3,3-d4acid sodium salt (TSP) (Cambridge Isotope Laboratories Inc). Two buffer solutions were prepared. Buffer solution A was a disodium phosphate buffer in H2O/D2O (80/20) with pH of 7.4 containing 6.15 mM NaN3 and 4.64 mM TSP. Buffer solution B was a disodium phosphate buffer in D2O (pH = 7.4) containing 1.5 M K2HPO4, 2 mM NaN3 and 4 mM of TSP. 96-well Ritter Deepwell plates were acquired from Novaveth B.V. and NMR tubes were purchased from Bruker Biospin Ltd.

The serum samples were thawed at 4°C and were mixed by inverting the tubes 10 times. Next, the samples (120 µL) were mixed with 120 µL of buffer solution A using a Gilson 215 liquid handler in combination with a Bruker SampleTrack system. For each sample,

190 µL of buffer-serum mixture was transferred into 3-mm SampleJet NMR tubes in 96 tube racks using a modified Gilson 215 tube filling station and kept at 6°C on a SampleJet sample changer while queued for acquisition.

The sample preparation of urine samples was performed using the method as described elsewhere [8, 9] with minor changes in the sample preparation step: 630 µL of urine from each sample were mixed with 70 µL buffer solution B; 565 µL of urine-buffer mixture were transferred to 5 mm SampleJet NMR tubes.

2-3 fecal pellets from each animal were weighed and mixed with milli-Q water at a ratio of ratio 1:5. The mixtures were homogenized by bead beating with zirconium oxide beads of 1 mm diameter for 3 min in a Bullet Blender 24 (Next Advance Inc., USA). The homogenized mixtures were centrifuged at 16100 x g for 20 min at 4 ^{o}C. The supernatants were carefully collected, and centrifugation was repeated under the same conditions. After the second centrifugation, 500 µL supernatant of each sample was taken for filtration.

The filters used for the filtration step were molecular weight cut-off (MWCO) filters Vivaspin 500 3kDa (GE Healthcare, UK). These filters need to be carefully washed prior to use in order to remove the significant glycerol contamination that was present in the unused filters. The washing procedure was as follows: the filters were centrifuged twice with 0.5 mL milli-Q water at 15000 x g for 20 min at 20^{o}C. Every time residual water was removed from the filters by allowing it to drain out properly. Eppendorf tubes were filled with 1 mL milli-Q water, after which the rinsed filters were inserted. 0.5 mL milli-Q water was added into the filter and the Eppendorf tubes were stored overnight at 4^{o}C. Then water was removed by centrifugation at 15000 x g for 20 min at 20^{o}C and the filters were rinsed again at the same conditions then residual water was removed from a filter by letting it drain. The filters were used immediately to avoid destroying of the membrane.

Using the washed filters, the supernatant of the second centrifugation of the feces-water mixture was then filtrated at 15000 x g for 20 min at 20 ^{o}C four times. Subsequently 150 µL filtrate was mixed with 30 µL milli-Q water and 20 µL buffer solution B. 190 µL of the mixture of each sample were transferred into 3 mm SampleJet NMR tubes.

The frozen liver, the spleen, the left kidney and samples of the three parts of the intestine (colon, jejunum and ileum) were weighed

and mixed with a 70 % methanol: 30 % milli-Q water mixture with the tissue:solvent ratio = 1:3. The mixtures were homogenized by applying 6 cycles of 1 min of bead beating and 1 min cooling on ice. For bead beating zirconium oxide beads of 1 mm diameter were used. The homogenized mixtures were centrifuged at 16100 x g for 20 min at 4 ^{o}C. The supernatants were collected and dried under a stream of nitrogen. Then, the dry residues were resuspended with D2O and then centrifugated at 16100 x g for 10 min at 4^{o}C. Buffer B was added to the supernatant for a final buffer concentration of 10%. The sample/buffer mixtures of liver, kidney, spleen, jejunum and ileum were transferred into 3mm SampleJet NMR tubes and colon samples were transferred into 1.7 mm SampleJet NMR tubes.

NMR data acquisition and spectral data processing

1H NMR data were collected using a Bruker 600 MHz AVANCE II spectrometer equipped with a 5 mm TCI cryogenic probe head and a z-gradient system. A Bruker SampleJet sample changer was used for sample insertion and removal. Two NMR protocols were used, one for the serum samples and one for all the others.

All experiments were recorded at 300 K, except the serum samples, which were recorded at 310K. A fresh sample of 99.8% methanol-d4 was used for temperature calibration [31]. The axial shims were optimized automatically before every measurement. Duration of 90° pulses were automatically calibrated for each individual sample using a homonuclear-gated mutation experiment [32] on the locked and shimmed samples after automatic tuning and matching of the probe head.

Four NMR experiments were performed on each serum sample: NOESY1D, CPMG, diffusion edited, and 2D JRES. The NOESY1D experiment was recorded using the first increment of a NOESY pulse sequence [33] with presaturation ($\gamma B1$ = 25 Hz) during a relaxation delay of 4 s and a mixing time of 10 ms for efficient water suppression [34]. 64 scans of 65,536 points covering a sweepwidth of 18,029 Hz were recorded and zero-filled to 65,536 complex points prior to Fourier transformation. A standard 1D Carr-Purcell-Meiboom-Gill (CPMG) pulse sequence with presaturation was used to for the acquisition of T2-filtered spectra. A pulse train of 128 refocusing pulses with individual spin echo delays of 0.6 ms was applied resulting in a total T2 filtering delay of 78 ms. After applying 4 dummy scans, a

total of 73,728 data points covering a spectral width of 12,019 Hz were collected. Otherwise the parameters were similar to the 1DNOESY experiment. The diffusion-edited spectrum was recorded with presaturation. The pulse sequence parameters were similar to those of the 1DNOESY experiment. An exponential window function was applied with a line-broadening factor of 1.0 Hz. After Fourier transformation, the spectra were automatically phase and baseline corrected and automatically referenced to the internal standard (TSP = 0.0 ppm). Afterwards, the spectra were referenced to the anomeric glucose doublet (5.23 ppm).

J-resolved spectra (JRES) were recorded with a relaxation delay of 2 s with presaturation (γB1 = 25 Hz) and 8 scans for each increment in the indirect dimension. A data matrix of 40 × 12,288 data points was collected covering a sweep width of 78 × 10,000 Hz. A sine-shaped window function was applied to both dimensions and the data was zero-filled to 256 × 16,384 complex data points prior to Fourier transformation. In order to remove the skew, the resulting data matrix was tilted along the rows by shifting each row (k) by 0.4992 ·(128-k) points and symmetrised about the central horizontal lines.

The NMR parameters were similar as for serum, except for the use of a stronger presaturation field (γB1 = 50 Hz). For the 1D experiments, 16 scans of 65536 points covering a sweepwidth of 12,336 Hz were accumulated, except for the colon and ileum samples, where 64 scans were used. Other parameters were similar as to those of the serum NOESY1D experiments. The 2D JRES experiments were also recorded with similar settings as to those of serum, with 2 scans per increment in the indirect dimension, and 8 scans per increment for colon and ileum.

Identification and quantification of the metabolites

Identification of small metabolites (< 1000 Da) was performed by exhausting search of the total 1D and 2D JRES data using the proprietary Bbiorefcode (Bruker Biospin Ltd.).

Quantification of the small metabolites and glycogen in liver samples was performed manually with the Chenomx NMR suite 8.1 software (Chenomx Inc.). Concentrations were extracted using the known TSP concentration (0.4 mM).

Serum lipoproteins and cholesterol were identified and quantified as described elsewhere [9].

GS-MS analysis of serum fatty acids

GC-MS quantitate analysis of medium- and long-chain fatty acids in serum samples was performed accordingly the protocol [30]. GC-MS quantitate analysis of serum short-chain fatty acids was performed accordingly the protocol [29].

Data analysis

All data analysis was performed with the R statistical environment (http://www.r-project.org/, R versions 3.6.0, 3.6.1). Basic data table handling was performed with a help of the tidyverse package (version 1.1.2); the data.Normalization function of the clusterSim (version 0.48-1) package was used for the data normalization before the modelling. For the evaluation of the principle source of variance on multi-block data and selection of the most relevant data blocks the Multi-Omics Factor Analysis (MOFA) package 1.2.0 and mixKernel (version 0.3) were used. To dissect an optimal subset of metabolites we used a regression approach, namely the DIABLO (Data Integration Analysis for Biomarker discovery using Latent variable approaches for 'Omics studies) tool of the mixOmics package (version 6.10.1). DIABLO combines a surprised multi-block modeling with variable selection. K-means clustering was computed using the standard of R command. For data visualization the ggplot2 package (version 3.2.1) was used.

Metabolic network enrichment analysis was performed in the MetExplore v2.23.15 environment, using the KEGG global network for a Chinese hamster (Cricetulus griseus) (a network for a golden Syrian hamster (Mesocricetus auratus) is not available currently) [35, 36]. The metabolites selected by the multi-block regression modeling were used for the pathway enrichment on each block separately. Only the pathways with $p<0.05$ after Bonferroni correction were included in the resulting graphs.

Acknowledgments

The research was supported by The Tomsk State University competitiveness improvement programme.

Supplementary information

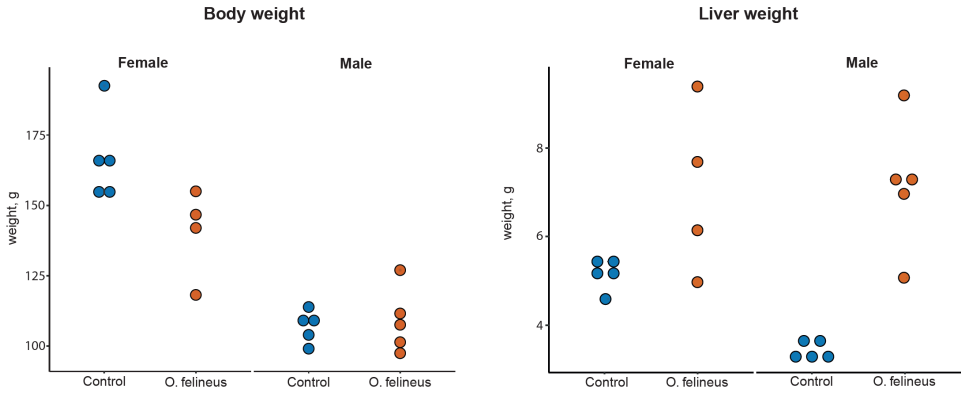

Supplementary Figure 1. The body and liver weights in the experimental animals. The values are presented separately for the female and male animals. A gender specific comparison shows that body weight of the infected female animals is significantly lower than non-infected ones (p-value = 0.04); liver weight of infected male animals is higher (p-value < 0.0001)

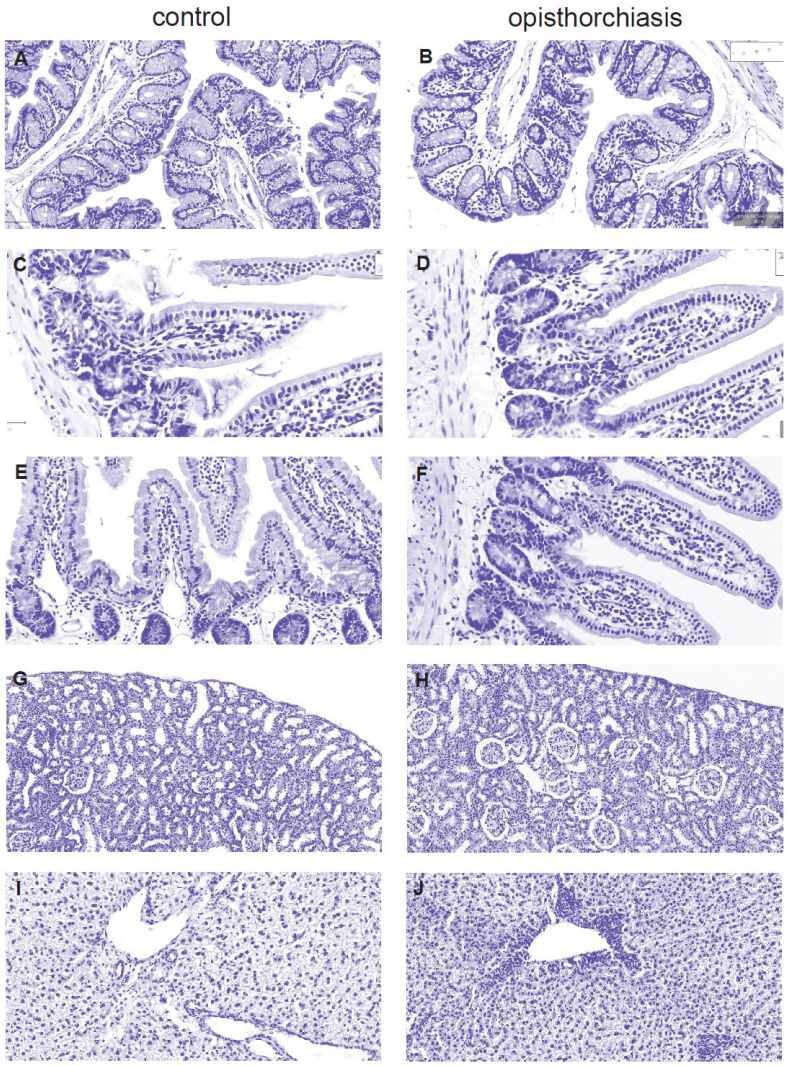

Supplementary Figure 2. Representative images of histological changes (hematoxylin and eosin staining) in investigated compartments. A: colon of the control animal, B: colon of the infected animal; C: ileum of the control animal, D: ileum of the infected animal; E: jejunum of the control animal, F: jejunum of the infected animal; G: kidney of the control animal, H: kidney of the infected animal; I: liver of the control animal, J: liver of the infected animal. There is no apparent difference between the segments of the digestive tract or the kidney of infected and uninfected groups. The liver samples of O. felineus infected animals had areas of inflammatory cell infiltration occurring around the bile ducts. The histological analysis of the liver samples of the control group showed no evidence of pathological changes in the liver or the bile ducts.

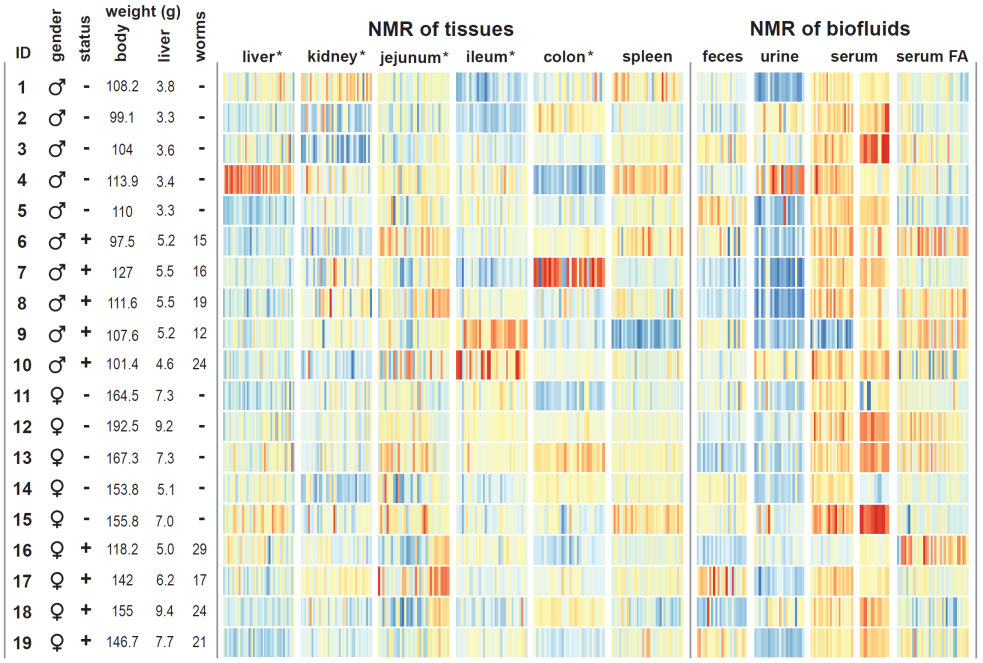

Supplementary Figure 3. A graphical summary of the entire data set.

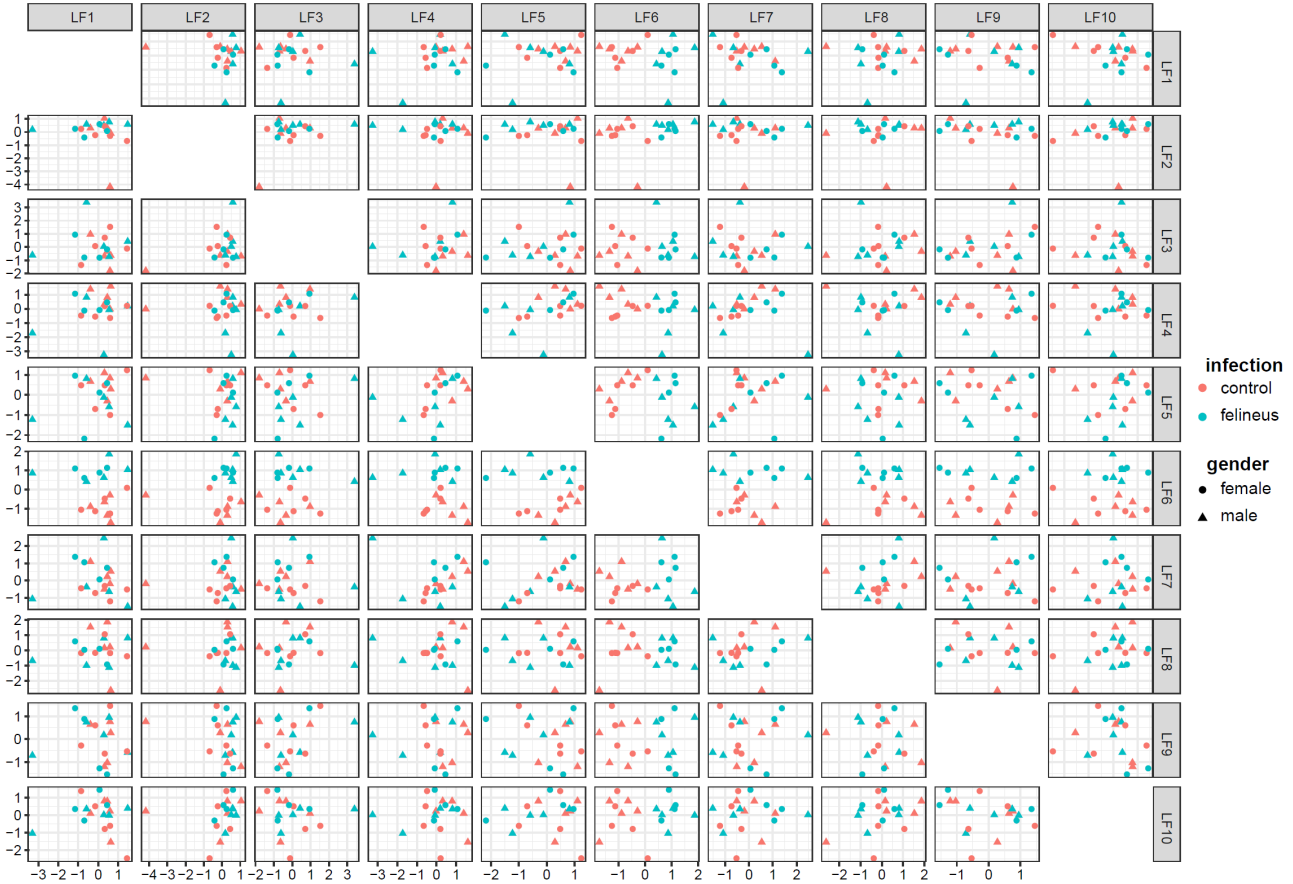

Supplementary Figure 4. MOFA factors scatter plot, pairwise combination of scatterplots between multiple factors. The plot was used to pinpoint a most relevant factor (F6)

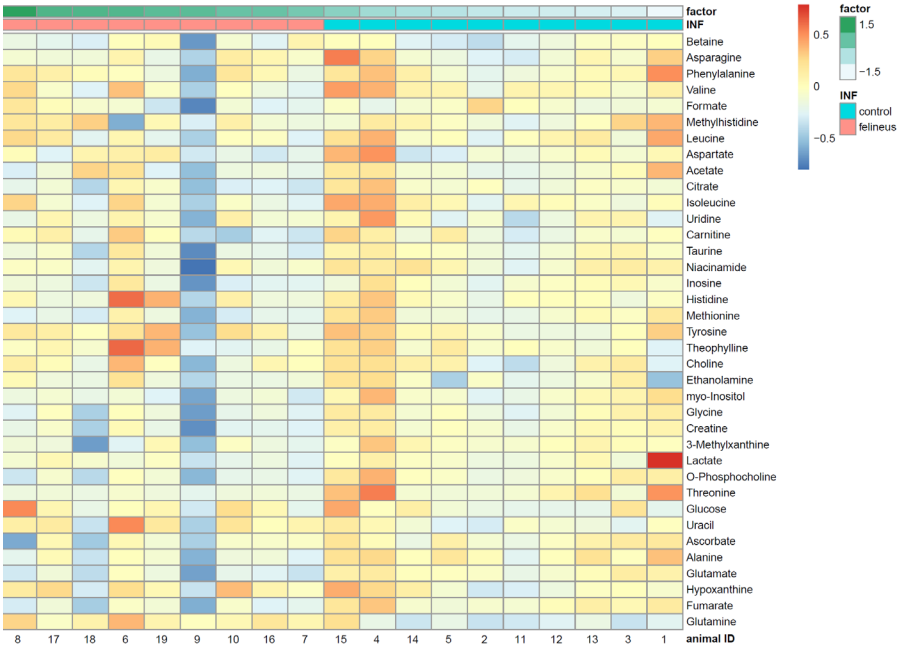

Supplementary Figure 5. Spleen. Heatmap of the normalized metabolites values. Samples are ordered by their factor values.

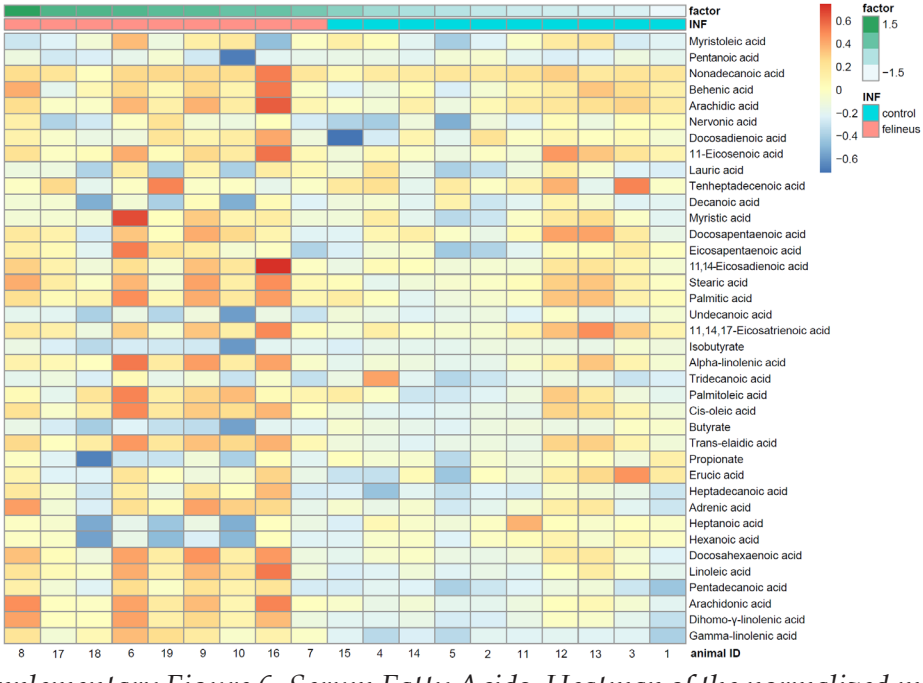

Supplementary Figure 6. Serum Fatty Acids. Heatmap of the normalized metabolites values. Samples are ordered by their factor values.

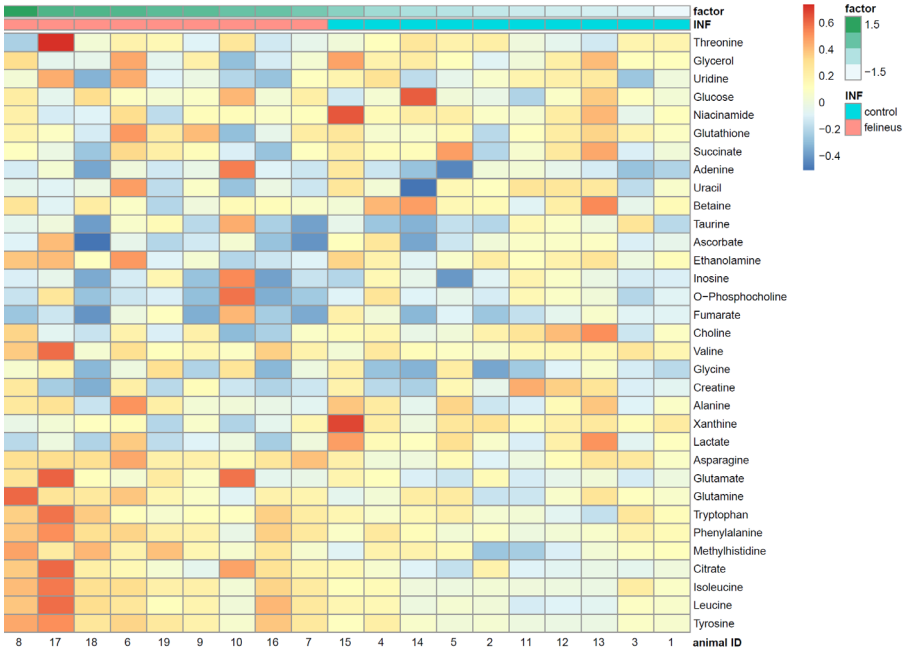

Supplementary Figure 7. Jejunum. Heatmap of the normalized metabolites values. Samples are ordered by their factor values.

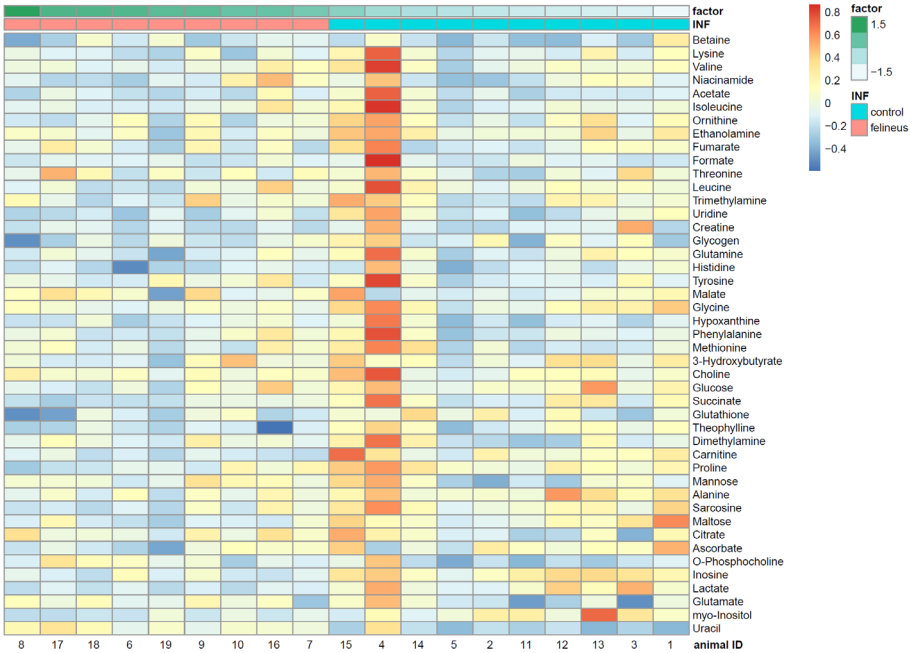

Supplementary Figure 8. Liver. Heatmap of the normalized metabolites values. Samples are ordered by their factor values.

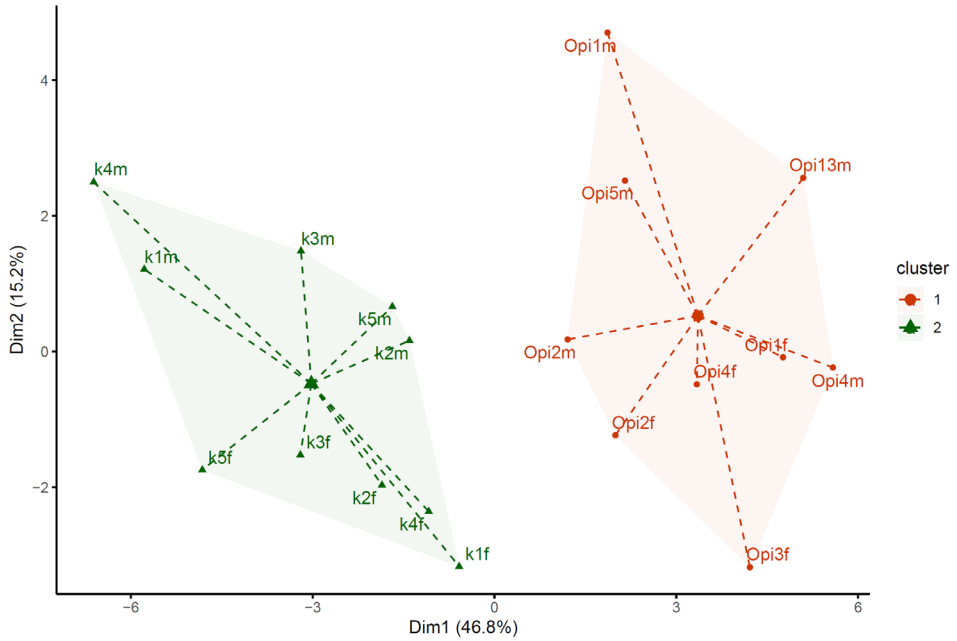

Supplementary Figure 9. K-means clustering solution built on the subset of the metabolites selected with a DIABLO (mixOmics) model.

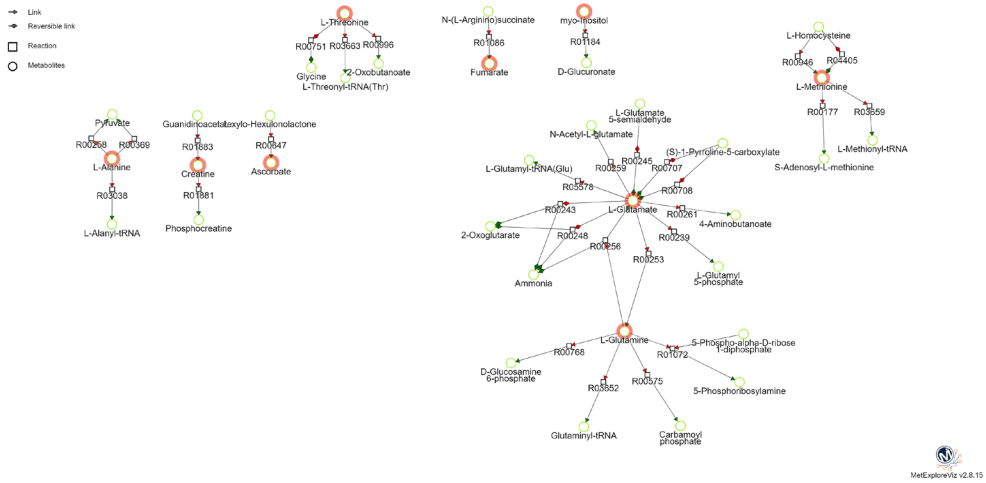

Supplementary Figure 10. The map of the metabolic networks of the spleen which could be associated with the O. felineus infection. MetExplore was used for mapping selected subsets of the metabolites into the pathways using organism specific database. Seven significant pathways involving were 30 reactions were chosen based on the Bonferroni-corrected p-values.

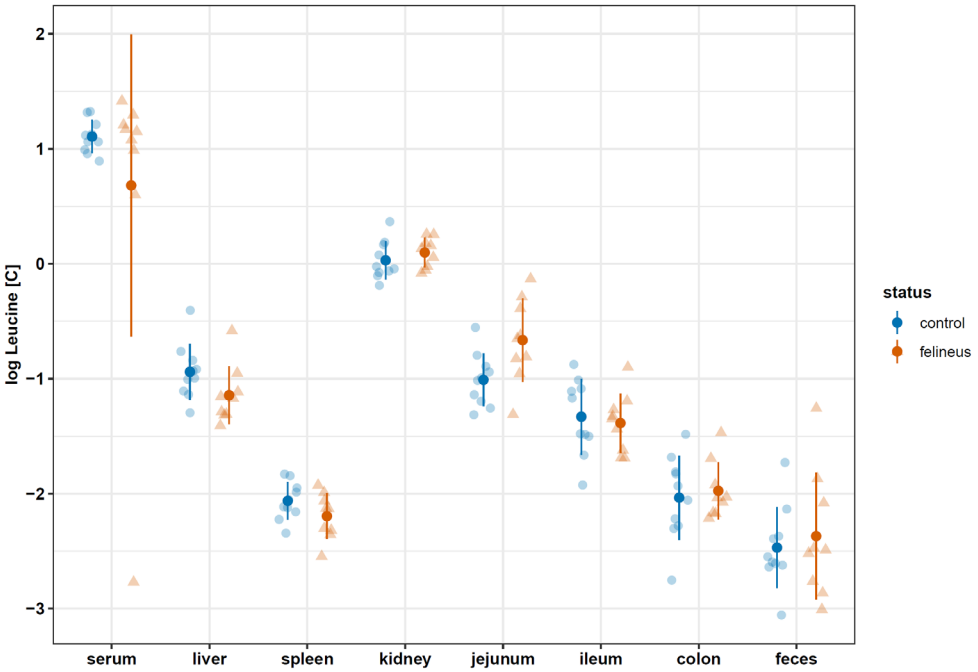

Supplementary Figure 11. Overview of the Leucine balance

Supplementary Table 1. 5-fold cross-validation AUC values and their respective p-values for each data block.

Block	cross-validated AUC	p-value
liver	0.922	0.0019
spleen	0.967	0.0002
jejunum	0.900	0.0033
serum fatty acids	1.000	0.0002

References

1. Petney TN, Andrews RH, Saijuntha W, Wenz-Mucke A, Sithithaworn P. The zoonotic, fish-borne liver flukes Clonorchis sinensis, Opisthorchis felineus and Opisthorchis viverrini. Int J Parasitol. 2013;43(12-13):1031-46.
2. Mairiang E, Mairiang P. Clinical manifestation of opisthorchiasis and treatment. Acta Tropica. 2003;88(3):221-7.
3. Pungpak S, Chalermrut K, Harinasuta T, Viravan C, Schelp PF, Hempfling A, et al. Opisthorchis viverrini infection in Thailand: symptoms and signs of infection--a population-based study. Trans R Soc Trop Med Hyg. 1994;88(5):561-4.
4. Liu LX, Harinasuta KT. Liver and intestinal flukes. Gastroenterol Clin North Am. 1996;25(3):627-36.
5. Humans IWGotEoCRt. Biological agents. Volume 100 B. A review of human carcinogens. IARC Monogr Eval Carcinog Risks Hum. 2012;100(Pt B):1-441.
6. Young ND, Nagarajan N, Lin SLJ, Korhonen PK, Jex AR, Hall RS, et al. The Opisthorchis viverrini genome provides insights into life in the bile duct. Nature Communications. 2014;5.
7. Young ND, Gasser RB. Opisthorchis viverrini Draft Genome - Biomedical Implications and Future Avenues. Asiatic Liver Fluke - from Basic Science to Public Health, Pt A. 2018;101:125-+.
8. Young ND, Campbell BE, Hall RS, Jex AR, Cantacessi C, Laha T, et al. Unlocking the Transcriptomes of Two Carcinogenic Parasites, Clonorchis sinensis and Opisthorchis viverrini. Plos Neglected Tropical Diseases. 2010;4(6).
9. Suttiprapa S, Sotillo J, Smout M, Suyapoh W, Chaiyadet S, Tripathi T, et al. Opisthorchis viverrini Proteome and Host-Parasite Interactions. Asiatic Liver Fluke - from Basic Science to Public Health, Pt B. 2018;102:45-72.
10. Mulvenna J, Sripa B, Brindley PJ, Gorman J, Jones MK, Colgrave ML, et al. The secreted and surface proteomes of the adult stage of the carcinogenic human liver fluke Opisthorchis viverrini. Proteomics.

2010;10(5):1063-78.
11. Kokova D, Mayboroda OA. Twenty Years on: Metabolomics in Helminth Research. Trends Parasitol. 2019.
12. Fedorova OS, Fedotova MM, Sokolova TS, Golovach EA, Kovshirina YV, Ageeva TS, et al. Opisthorchis felineus infection prevalence in Western Siberia: A review of Russian literature. Acta Tropica. 2018;178:196-204.
13. Keiser J, Utzinger J. Foodborne trematodiases. Clin Microbiol Rev. 2009;22(3):466-83.
14. Pomaznoy MY, Logacheva MD, Young ND, Penin AA, Ershov NI, Katokhin AV, et al. Whole transcriptome profiling of adult and infective stages of the trematode Opisthorchis felineus. Parasitology International. 2016;65(1):12-9.
15. Kokova DA, Kostidis S, Morello J, Dementeva N, Perina EA, Ivanov VV, et al. Exploratory metabolomics study of the experimental opisthorchiasis in a laboratory animal model (golden hamster, Mesocricetus auratus). PLoS Negl Trop Dis. 2017;11(10):e0006044.
16. Rodrigues MV, de Castro SO, de Albuquerque CZ, Mattaraia VGD, Santoro ML. The gingival vein as a minimally traumatic site for multiple blood sampling in guinea pigs and hamsters. Plos One. 2017;12(5).
17. Diehl KH, Hull R, Morton D, Pfister R, Rabemampianina Y, Smith D, et al. A good practice guide to the administration of substances and removal of blood, including routes and volumes. J Appl Toxicol. 2001;21(1):15-23.
18. Verhoeven A, Slagboom E, Wuhrer M, Giera M, Mayboroda OA. Automated quantification of metabolites in blood-derived samples by NMR. Analytica Chimica Acta. 2017;976:52-62.
19. Wu DH, Chen AD, Johnson CS. An Improved Diffusion-Ordered Spectroscopy Experiment Incorporating Bipolar-Gradient Pulses. Journal of Magnetic Resonance Series A. 1995;115(2):260-4.
20. Verhoeven A, Giera M, Mayboroda OA. KIMBLE: A versatile visual NMR metabolomics workbench in KNIME. Analytica Chimica Acta. 2018;1044:66-76.
21. De Meyer T, Sinnaeve D, Van Gasse B, Tsiporkova E, Rietzschel ER, De Buyzere ML, et al. NMR-based characterization of metabolic alterations in hypertension using an adaptive, intelligent binning algorithm. Analytical Chemistry. 2008;80(10):3783-90.
22. Dieterle F, Ross A, Schlot-

terbeck G, Senn H. Probabilistic quotient normalization as robust method to account for dilution of complex biological mixtures. Application in H-1 NMR metabonomics. Analytical Chemistry. 2006;78(13):4281-90.
23. Smilde AK, Jansen JJ, Hoefsloot HCJ, Lamers RJAN, van der Greef J, Timmerman ME. ANOVA-simultaneous component analysis (ASCA): a new tool for analyzing designed metabolomics data. Bioinformatics. 2005;21(13):3043-8.
24. Stekhoven DJ, Buhlmann P. MissForest--non-parametric missing value imputation for mixed-type data. Bioinformatics. 2012;28(1):112-8.
25. Mallol R, Rodriguez MA, Brezmes J, Masana L, Correig X. Human serum/plasma lipoprotein analysis by NMR: Application to the study of diabetic dyslipidemia. Progress in Nuclear Magnetic Resonance Spectroscopy. 2013;70:1-24.
26. Smilde AK, Westerhuis JA, Hoefsloot HCJ, Bijlsma S, Rubingh CM, Vis DJ, et al. Dynamic metabolomic data analysis: a tutorial review. Metabolomics. 2010;6(1):3-17.
27. Kaewpitoon N, Kaewpitoon SJ, Pengsaa P, Sripa B. Opisthorchis viverrini: The carcinogenic human liver fluke. World J Gastroentero. 2008;14(5):666-74.
28. Mel'nikov V, Skarednov NI. Clinical aspects of acute opisthorchiasis in the nonnative population of the northern Ob region. Med Parazitol (Mosk). 1979;48(5):12-6.
29. WHO. Opisthorchiasis felinea [Available from: https://www.who.int/foodborne_trematode_infections/opisthorchiasis/Opisthorchiasis_felinea/en/.
30. Saric J, Li JV, Wang Y, Keiser J, Veselkov K, Dirnhofer S, et al. Panorganismal metabolic response modeling of an experimental Echinostoma caproni infection in the mouse. J Proteome Res. 2009;8(8):3899-911.
31. Saric J, Li JV, Wang Y, Keiser J, Bundy JG, Holmes E, et al. Metabolic profiling of an Echinostoma caproni infection in the mouse for biomarker discovery. PLoS Negl Trop Dis. 2008;2(7):e254.
32. Weinstein MS, Fried B. The Expulsion of Echinostoma-Trivolvis and Retention of Echinostoma-Caproni in the Icr Mouse - Pathological Effects. International Journal for Parasitology. 1991;21(2):255-7.
33. Wu JF, Holmes E, Xue J, Xiao SH, Singer BH, Tang HR, et al. Metabolic alterations in the hamster co-infected with

Schistosoma japonicum and Necator americanus. Int J Parasitol. 2010;40(6):695-703.
34. Pershina AG, Ivanov VV, Efimova LV, Shevelev OB, Vtorushin SV, Perevozchikova TV, et al. Magnetic resonance imaging and spectroscopy for differential assessment of liver abnormalities induced by Opisthorchis felineus in an animal model. Plos Neglected Tropical Diseases. 2017;11(7).
35. Kostidis S, Kokova D, Dementeva N, Saltykova IV, Kim HK, Choi YH, et al. (1)H-NMR analysis of feces: new possibilities in the helminthes infections research. BMC Infect Dis. 2017;17(1):275.
36. Jimenez B, Holmes E, Heude C, Tolson RF, Harvey N, Lodge SL, et al. Quantitative Lipoprotein Subclass and Low Molecular Weight Metabolite Analysis in Human Serum and Plasma by (1)H NMR Spectroscopy in a Multilaboratory Trial. Anal Chem. 2018;90(20):11962-71.
37. Barrilero R, Gil M, Amigo N, Dias CB, Wood LG, Garg ML, et al. LipSpin: A New Bioinformatics Tool for Quantitative (1) H NMR Lipid Profiling. Anal Chem. 2018;90(3):2031-40.
38. Wu J, Xu W, Ming Z, Dong H, Tang H, Wang Y. Metabolic changes reveal the development of schistosomiasis in mice. PLoS Negl Trop Dis. 2010;4(8).
39. Laothong U, Pinlaor P, Boonsiri P, Hiraku Y, Khoontawad J, Hongsrichan N, et al. alpha-Tocopherol and lipid profiles in plasma and the expression of alpha-tocopherol-related molecules in the liver of Opisthorchis viverrini-infected hamsters. Parasitology International. 2013;62(2):127-33.
40. Changbumrung S, Ratarasarn S, Hongtong K, Migasena P, Vutikes S, Migasena S. Lipid-Composition of Serum Lipoprotein in Opisthorchiasis. Annals of Tropical Medicine and Parasitology. 1988;82(3):263-9.
41. Hardardottir I, Grunfeld C, Feingold KR. Effects of endotoxin and cytokines on lipid metabolism. Curr Opin Lipidol. 1994;5(3):207-15.
42. Kitagawa S, Yamaguchi Y, Imaizumi N, Kunitomo M, Fujiwara M. A uniform alteration in serum lipid metabolism occurring during inflammation in mice. Jpn J Pharmacol. 1992;58(1):37-46.
43. Sherman DR, Guinn B, Perdok MM, Goldberg DE. Components of sterol biosynthesis assembled on the oxygen-avid hemoglobin of Ascaris. Science. 1992;258(5090):1930-2.